Seismic Signal and Noise Separation on Downhole Distributed Acoustic Sensing at SAFOD

Siyuan Yuan, Weiqiang Zhu, Xiaoxi Zeng, Ruiming Zhu, Ariel Lellouch, Biondo Biondi

ABSTRACT

Distributed Acoustic Sensing (DAS) is an emerging technology that is promising in monitoring earthquakes with a low cost per sensor, high spatial and temporal resolution, and the ability to cover a long distance with a single interrogator. We implement neural networks to denoise earthquakes recorded in a vertical array. We implement a U-Net based model with an encoder-decoder structure, which is trained to learn simultaneously a sparse representation of the data and a non-linear function mapping the representation to masks of signal and noise. The masks are used for signal separation. To train our networks, we synthesize clean DAS data using 1-D geophone data with high signal-to-noise ratio recorded by North California Seismic Network. The models are trained on 180,000 synthetic clean-noisy pairs. Using the signal-to-noise ratio as a denoising metric, we show that our network significantly removes noise while minimally altering the signal waveforms for all five randomly chosen synthetic and field datasets.

INTRODUCTION

Earthquake signal denoising is of great interest in seismology as it offers the possibility to improve recorded data quality. All subsequent analysis, such as earthquake detection and location, will benefit from this improvement. Traditionally, 3 components (3-C) geophones are used to record earthquakes. Zhu et al. (2018) showed that single-component geophone signals can be denoised using deep learning models. Over the last decade, the new technology of distributed acoustic sensing (DAS) has been emerging as a possible alternative. DAS uses a fiber-optic cable with an interrogator to measure the strain or strain rate, along the fiber. This allows for surface or subsurface monitoring with dense spatial sampling. It has been shown to be useful for both active surveys and passive monitoring, onshore and offshore, and with the fiber installed either downhole or horizontally (Ajo-Franklin et al., 2017; Biondi et al., 2017; Daley et al., 2013, 2016; Dou et al., 2017; Hornman, 2017; Jousset et al., 2018; Karrenbach et al., 2017; Lindsey et al., 2017; Martin et al., 2017a,b; Martin and Biondi, 2018; Mateeva et al., 2014, 2013; Wang et al., 2018; Lellouch et al., 2019). Moreover, the cost per sensor for DAS is much lower than that of traditional geophone arrays. DAS is also able to cover long distances (tens of kilometers) measurement with a single interrogator, thanks to low cost. However, DAS records might be contaminated

with strong ambient noise and instrument noise. Herein, we apply deep learning to denoise such records.

A DAS record has two dimensions, one corresponding to the time and the other to the trace number (spatial location). The input to our neural network is the Short Time Fourier Transform (STFT) along the time axis. The STFT results are in three dimensions (time, frequency and trace number) and have two channels (real and imaginary part). The outputs are two masks in the STFT domain corresponding to the recovered signal and noise, respectively. Each pixel of the masks has a value between zero and one, with zero representing pure noise and one representing pure signal.

NETWORK ARCHITECTURES

The U-Net architecture has been shown to be fast and precise in bio-medical image segmentation (Ronneberger et al., 2015). Zhu et al. (2018) used the U-Net architecture with an encoder-decoder structure to develop a deep learning denoiser for 1-D time series of traditional geophone data. The authors trained their neural network on various types of noise and earthquake signals. They demonstrated that with their deep U-Net neural network, a better signal-to-noise (SNR) ratio has been achieved compared to traditional denoising approaches (normal spectral filtering). In this study, we also aim at denoising earthquake recordings. However, in our study, we only have one hundred earthquakes, all contaminated with noise. This is a unique difficulty, not shared by Zhu et al. (2018) and similar studies. In addition, unlike 1-D geophone signals, we have many more (800) traces along the fiber to record earthquakes at the same time. Our network should be able to learn spatial patterns, arising from the subsurface velocity structure and earthquake location (Lellouch et al., 2019), which is not required for 1-D geophone denoising networks.

DATASET AND FEATURES

The DAS fiber we use in this study is located in the vicinity of the San Andreas Fault. A detailed description of the SAFOD experiment can be found in Zoback et al. (2011). The fibers are under tension of approximately 1N and housed in a 0.9mm steel tube cemented between casing strings. Lellouch et al. (2019) use Figure 1 to illustrate the area of the well. In the depth range of interest, the well is deviating north. Data are collected with a fiber down to a depth of 864 m in the subsurface, organized by William Ellsworth. Due to a failure of the loop at the end of the fiber, we limit our analysis to a depth of 800 m. Along this depth, we have 800 traces with 1 m spacing continuously monitoring seismic waves during three weeks from June 21, 2017 to July 10, 2017. During this period, about 100 earthquakes occurred within a radius of 140 km away from the fiber. Figure 2 shows an example of a SAFOD earthquake recording. The vertical axis is depth along the fiber from ground down

to 800 m. The horizontal axis depicts time. The temporal sampling rate of the data is 100 Hz after downsampling with an anti-alias filter.

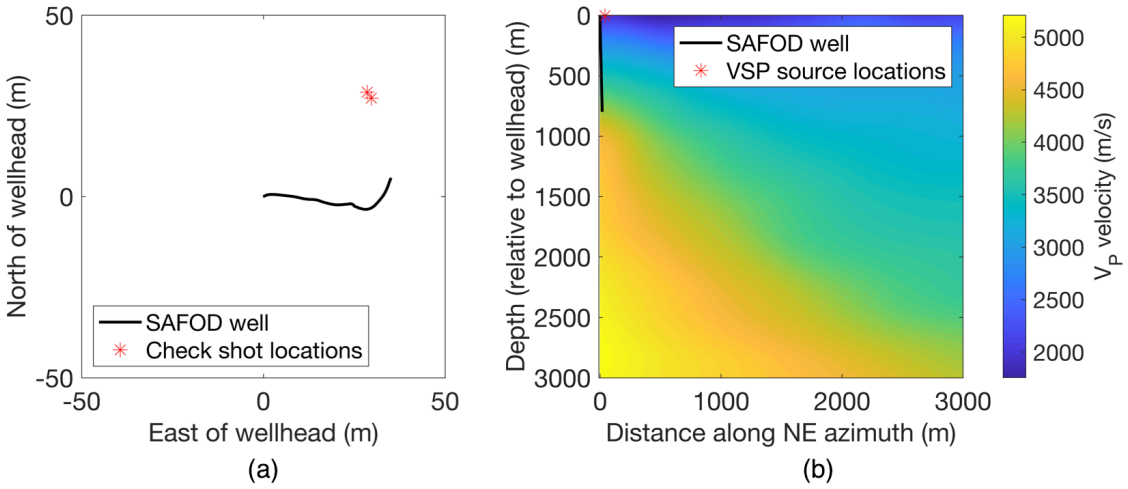

Figure 1: The SAFOD borehole in map (a) and side (b) views from Lellouch et al. (2019). The side view is along the NE azimuth, which is perpendicular to the San Andreas Fault. The well trajectory is plotted as a black line.A 2-D line crossing the fault zone and taken along the NE azimuth from a regional P-wave velocity model (Hole et al., 2006) is displayed in the background. Source locations plotted as red stars are for a geophone survey, which is irrelevant to this study. [**NR**]

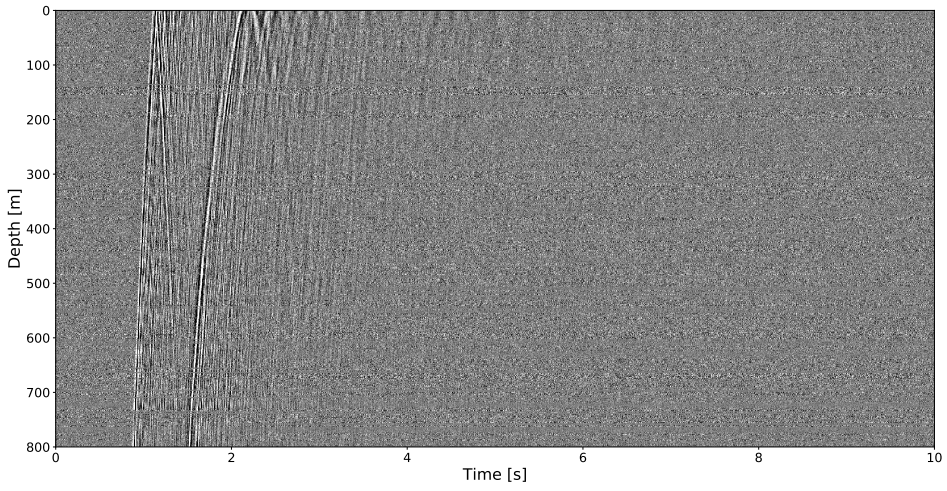

Figure 2: An example of SAFOD earthquake recordings. The vertical axis is depth along the fiber from ground down to 800 m. There are 800 traces with 1 m spacing. [ER]

Since we do not have a clean DAS signal and DAS signals are assumed to share similarities in waveforms with geophone data, we synthesize clean DAS signals by shifting geophone signals along the depth according to the P and S wave velocity models along the fiber given by Lellouch et al. (2019). As coherent moveouts along the depth distinguishes earthquakes from noise, learning moveout patterns can be helpful for our network to separate signal from noise. The geophone datasets we used were recorded from 2014 to 2018 by high broadband channels (HNZ) of the North California Seismic Network. In total, we use 18,000 geophone recordings, and for each of them, we simulated ten random cases where waves hit the fiber at random incidence angles in order to let our network learn various moveout patterns. To mimic a real DAS signal, for each random case, We add small perturbations to the velocity-model based computed arrival times. In addition, we randomly removed signal from some randomly chosen traces, and added random amplitude factors for each trace. Figure 3 shows an example of the synthetic DAS data using one of the geophone datasets. We added randomly chosen noise data from our field dataset to the synthetic clean signal to synthesize noisy data. We preprocessed the recordings by performing the STFT and we normalized our data for each of the 800 traces by their corresponding L-2 norms. In order to let neural networks learn different shifted versions of the signal and different noise levels, for each of the 100 iterations, we randomly windowed 20 seconds of those 50 second recordings and randomly select 20 seconds noise from our three-week recordings to produce synthetic data. We selected the hyperparameters based on the performance on the 180 validation synthetic datasets. We used 5 randomly chosen test data and field data to evaluate the performance of our model.

METHOD

Convolution Neural Networks (CNN) encoder-decoder architecture is able to learn efficient representations in computer vision tasks. Our encoder network maps the preprocessed 3-D STFT spectrum, which contains two channels (real and imaginary parts), to low-dimension features. The decoder network maps these features to generate an output with the original dimension. Since the outputs are signal and noise masks with elements between zero and one, our task is equivalent to predicting the probability of being a signal for each pixel of the inputs. Thus, we adopt an image segmentation approach. We use the cross-entropy loss function to optimize our model:

$$L(p, y) = -[ylog(p) + (1 - y)log(1 - p)]$$

where y is the ground truth signal mask. We denote the STFT transforms of the ground truth signal and noise recorded by trace x and at time t as $S(x, t, f)$ and $N(x, t, f)$, respectively. y can be computed as

$$y(x, t, f) = \frac{1}{1 + \frac{|N(x,t,f)|}{|S(x,t,f)|}}$$

and p in the loss function is the predicted signal mask. The closer p matches y, the lower the loss function is.

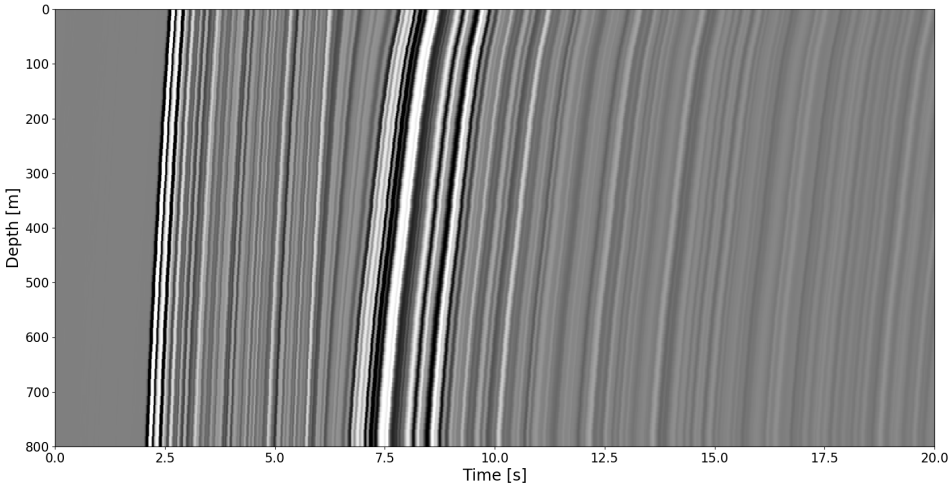

(a)

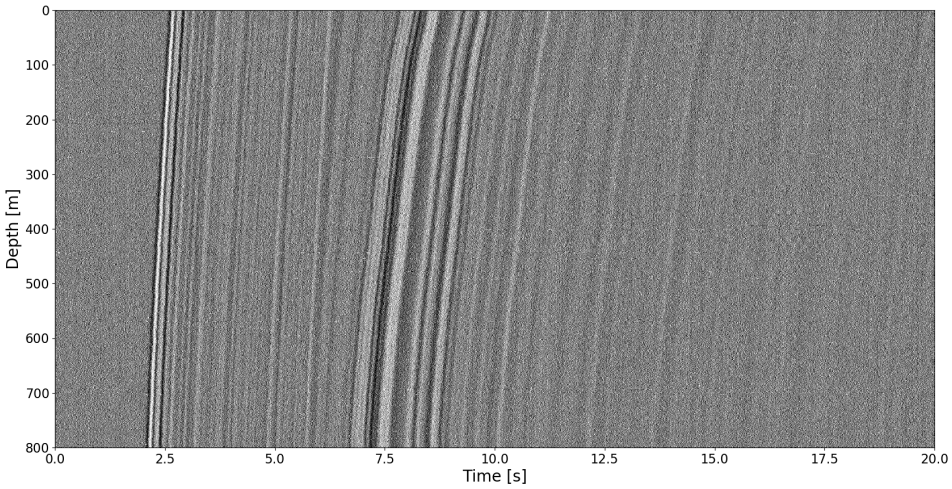

(b)

Figure 3: An example of the synthetic DAS data using one of the geophone data shifted along the depth according to the estimated velocity model by Lellouch et al. (2019). (a) Synthetic clean data; (b) Synthetic data contaminated by a randomly chosen DAS recording of noise. [ER]

U-Net based architecture

The U-Net based architecture consists of a series of fully convolutional layers with 10 descending encoding and 10 ascending decoding layers. Skip connections were implemented to improve the convergence of training and prediction performance by

passing low-level features into the decoder. Figure 4 shows the U-Net architecture.

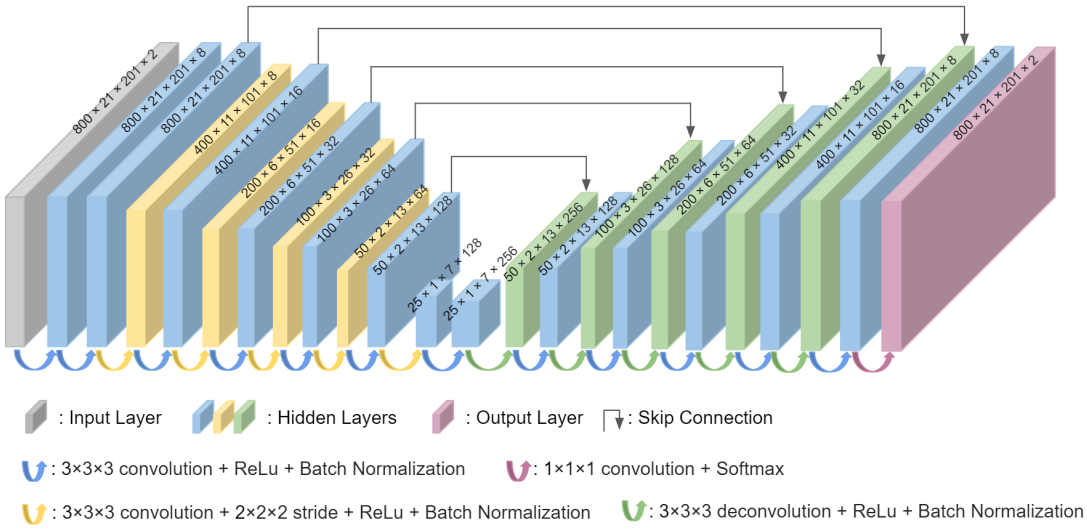

Figure 4: U-Net Based Network Architecture [NR]

EXPERIMENTS/RESULTS/DISCUSSION

Hyperparameter tuning

For the U-Net based model, we test three different learning rates, 10^{-2}, 10^{-3} and 10^{-4}, with the same decay rate of 0.95. Our GPU V100 memory can only fit a maximum batch size of two. As a result, we tried both batch sizes of two and stochastic gradient descent. In total, six models, named from Unet1 to Unet6, with different sets of hyperparameters are tested. To avoid overfitting, we added dropout for Unet1 and Unet5. When training them, we added pure noise in the training set to let the networks learn noise patterns. Table 1 shows both training and validation loss for all the five models. Among the six, Unet1 performs the best with the lowest training and validation loss. We find that a higher learning rate tends to fasten convergence and results in a lower training error. A batch size of two helps convergence because of the batch norm technique we implemented in our U-Net. Comparisons of Unet1 and Unet4 show that dropout decreases variance. Similarly, dropout brings down the variance of Unet5 compared to Unet6. The validation and training loss for Unet1 is the close, which indicates that Unet1 does not overfit the training data. We chose Unet1 as our best model, which has a test loss of 0.347. Figure 5 shows an example of denoising results for a synthetic data in the validation set. As can be seen, signal and noise are well separated.

Table 1: U-Net Based Model Performance

Model	**Hyper-Parameters**				**Loss**	
	Learning Rate	**Batch Size**	**Dropout**	**Include Zero Signal**	**Training**	**Valid**
Unet1	10^{-2}	2	0.2	Yes	0.318	0.336
Unet2	10^{-4}	2	0	No	0.342	0.441
Unet3	10^{-3}	2	0	No	0.320	0.661
Unet4	10^{-2}	2	0	No	0.321	0.723
Unet5	10^{-2}	1	0.2	Yes	0.337	3.077
Unet6	10^{-2}	1	0	No	0.340	174.427

Model evaluation

We choose the signal-to-noise ratio (SNR) to evaluate the performance of our model. The SNR is calculated as

$$SNR = 10log_{10}(\sigma_{signal}/\sigma_{noise})$$

where σ_{signal} and σ_{noise} are, respectively the standard deviations of waveforms before and after the first arrival. We choose a total variation denoising algorithm as our baseline method. The total variation method aims at minimizing the total variation of the image, which is defined as the integral of the norm of the image. This code we used is an implementation of the algorithm of Rudin, Fatemi and Osher that was proposed by Chambolle (2004). Two field earthquake recordings, named event1 and event2, are used to test the performance of our model in the real world. Table 2 shows their metadata from the USGS catalog. Figure 6 shows the denoising results for event1. In Figure 7, we show the time and STFT representations of a single data trace. Signal is well recovered with Unet1. In Figure 6 panel (iii), we can see slight signal moveout left in the residual, which could indicate that our network is not well trained enough to be generalized to event1. Figure 8 shows the results of the total variation method. Comparing with Figure 6, we can see that U-Net has weaker signal leakage than the total variation approach. U-Net performs better in removing the noise before the earthquake arrival (around 1 s). Figure 9 and 10 show the denoising results for event2 with Unet1. Figure 11 shows the results of the total variation method. Unet also performs better than the total variation method with a less signal leakage problem and more noise energy are removed from recovered signal. Figure 12 shows one trace of the data in Figure 11 in time and STFT domain. Compared to Figure 10, we show that our network not only performs better at recoving moveout along the depth, but also is better at preserving waveforms than the total variation method. In Table 3, we show and compare the SNRs before and after denoising with the two models on two field datasets and three randomly selected validation datasets. The recovered signals by the U-Net model have higher SNRs of the three validation datasets than those recovered by the baseline method by a factor of 5.4, on average.

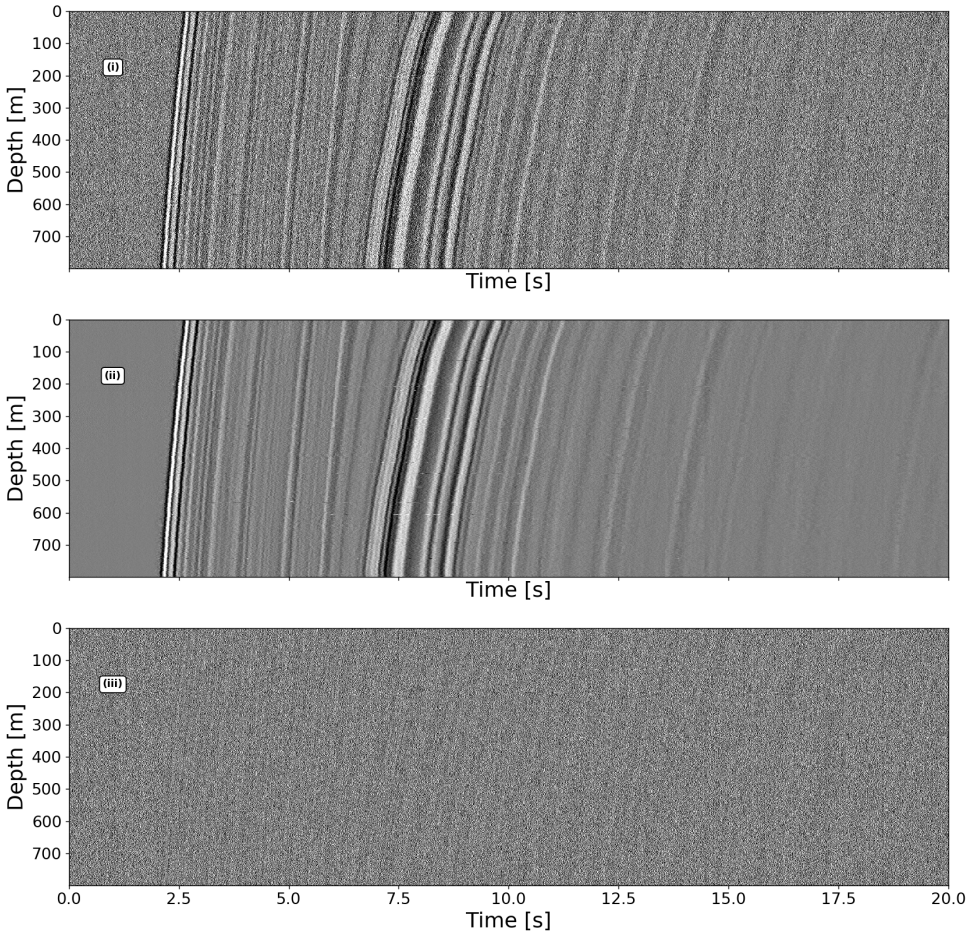

Figure 5: Denoising performance on a synthetic seismogram. The noisy signal is plotted in panel (i). Panel (ii) shows the denoised signal. The recovered noise is shown in panel (iii). [CR]

For the two field datasets, the average factor is 1.8. In all five cases, U-Net achieves better SNRs of the recovered signal.

Table 2: Meta data of the two events recorded by the DAS array

Event	**Date**	**Magnitude**	**Depth (km)**	**DistanceToDAS (km)**
event1	July 10, 2017	1.12	3.8	5.2
event2	July 03, 2017	1.66	0.68	12.4

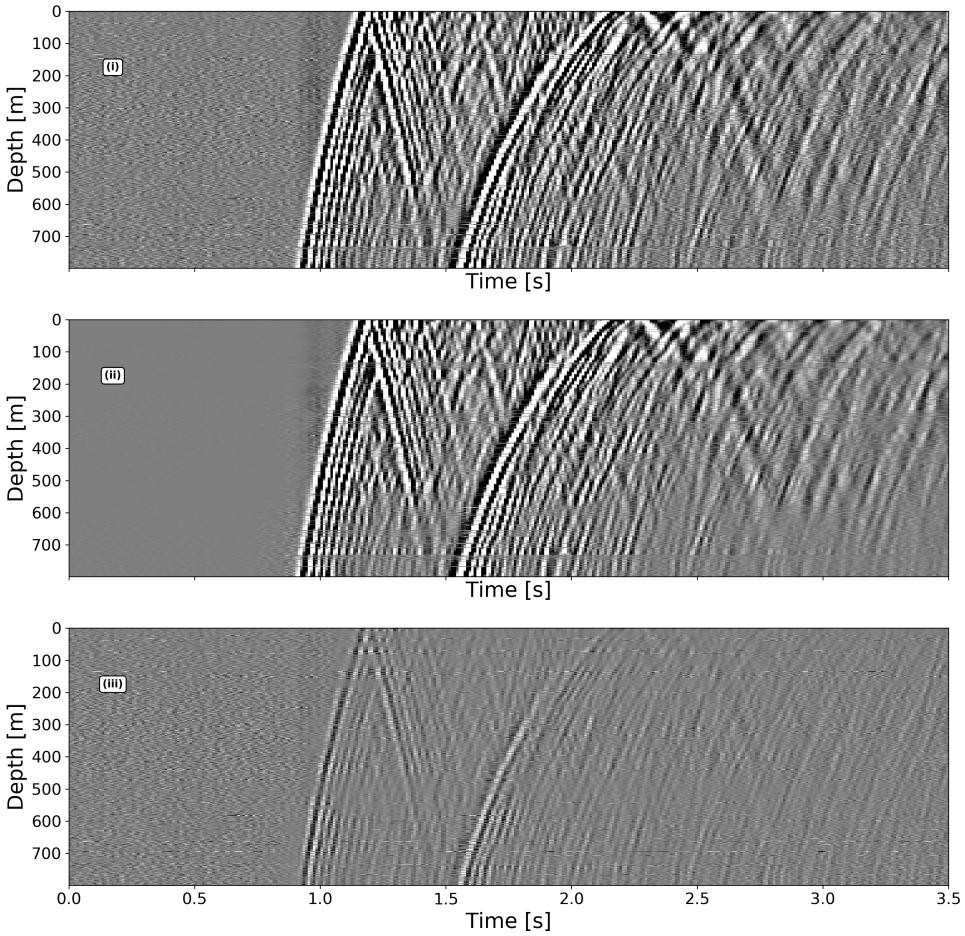

Figure 6: Denoising performance of the U-Net model on event1. The noisy signal is plotted in panel (i). Panel (ii) shows the denoised signal. The recovered noise is shown in panel (iii). We see slight signal moveout patterns in panel (iii), which could indicate that our network is not well trained enough to be generalized to event1. [CR]

CONCLUSIONS

We implement a U-Net architecture to denoise DAS recordings. A total variation denoising algorithm is chosen as the baseline model. We compared the performances of the two models on five randomly selected synthetic and field datasets. The recovered signals by the U-Net model have higher SNRs of the three validation datasets than those by the baseline model, on average, by a factor of 5.4. The factor for the two field datasets is 1.8. In all five cases, U-Net achieves better SNRs of the recovered

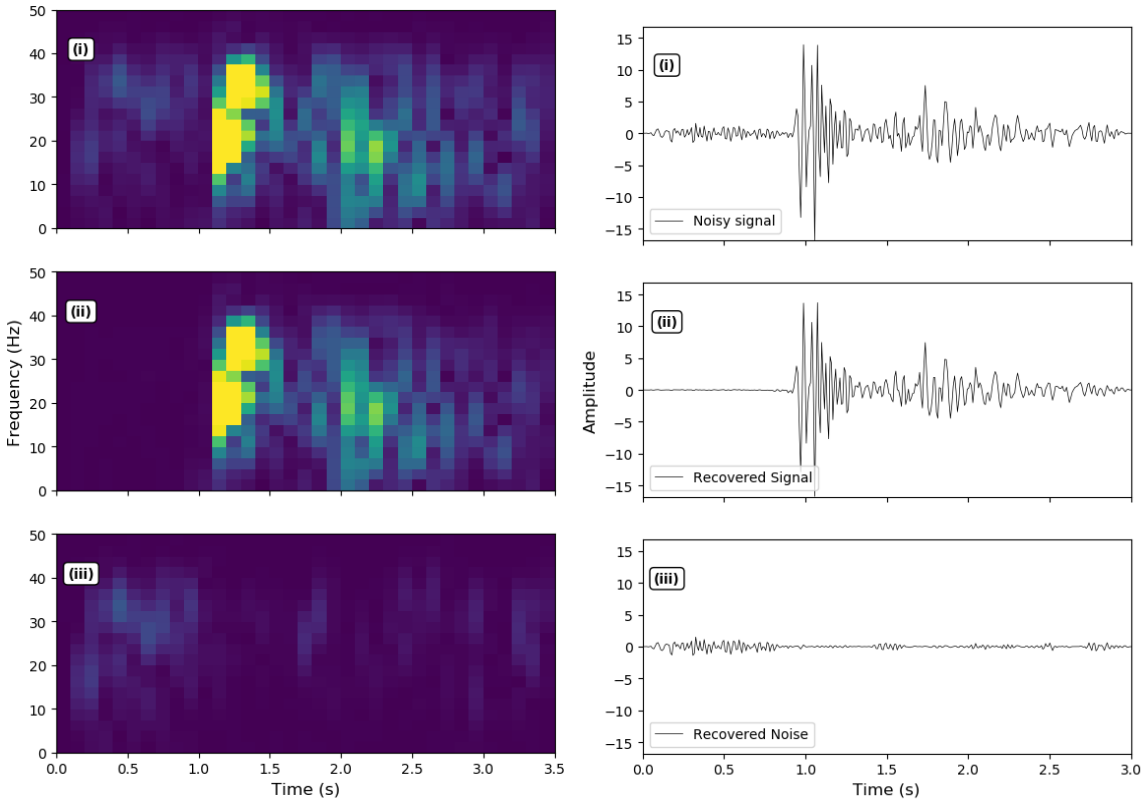

(a) (b)

Figure 7: Denoising performance of Unet1 on event1, trace #100 at a depth of 100 m of seismograph shown in Figure 6. Ground truth clean signal, noise, and noisy signal in time-frequency (a) and time (b) domain are plotted in panels (i) (ii) (iii). [CR]

Table 3: SNR (dB) Performance With Baseline and Best Model

Data set	**Noisy Signal SNR**	**Denoised Signal SNR**	**Baseline Model SNR**
Validation Data1	3. 78	18.18	3.72
Validation Data2	1.87	18.46	3.31
Validation Data3	0.84	14.46	2.50
event1	6.52	15.96	11.95
event2	2.57	10.17	4.35

signal. For future work, we could use more synthetic data to train our models, so that new models learn more general cases to achieve weaker signal leakage on field data.

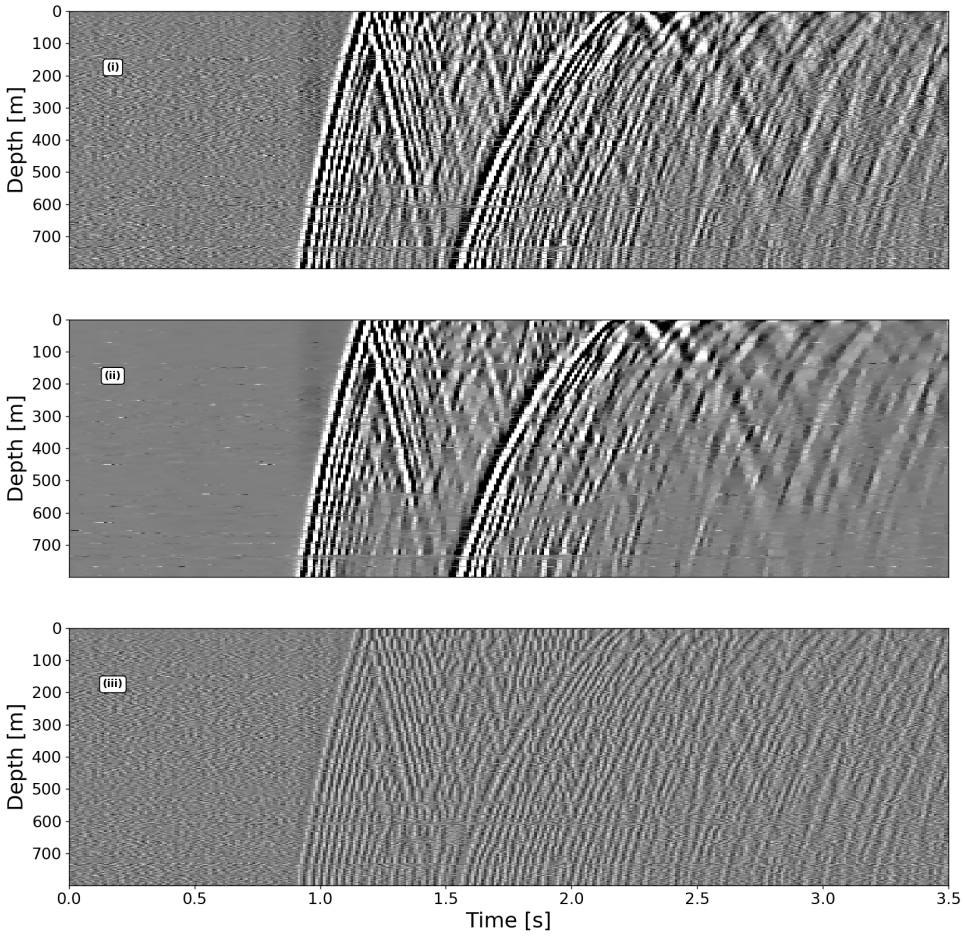

Figure 8: Denoising performance of the total variation method on a event1. The noisy signal is plotted in panel (i). Panel (ii) shows the denoised signal. The recovered noise is shown in panel (iii). We show less noise energy is filtered out in panel (ii), and stronger signal energy is left in panel (iii) compared to Figure 6. [ER]

ACKNOWLEDGEMENTS

We thank Center for Computational Earth and Enviromental Science (CEES) for computational resources. We thank Stanford Center for Induced and Triggered Seismicity (SCITS) and OptoSense for providing us with the DAS recordings. We thank Stanford Exploration Project (SEP) affiliates for funding. Geophone data used for synthesizing DAS recordings were accessed through the Northern California Earthquake Data Center (NCEDC).

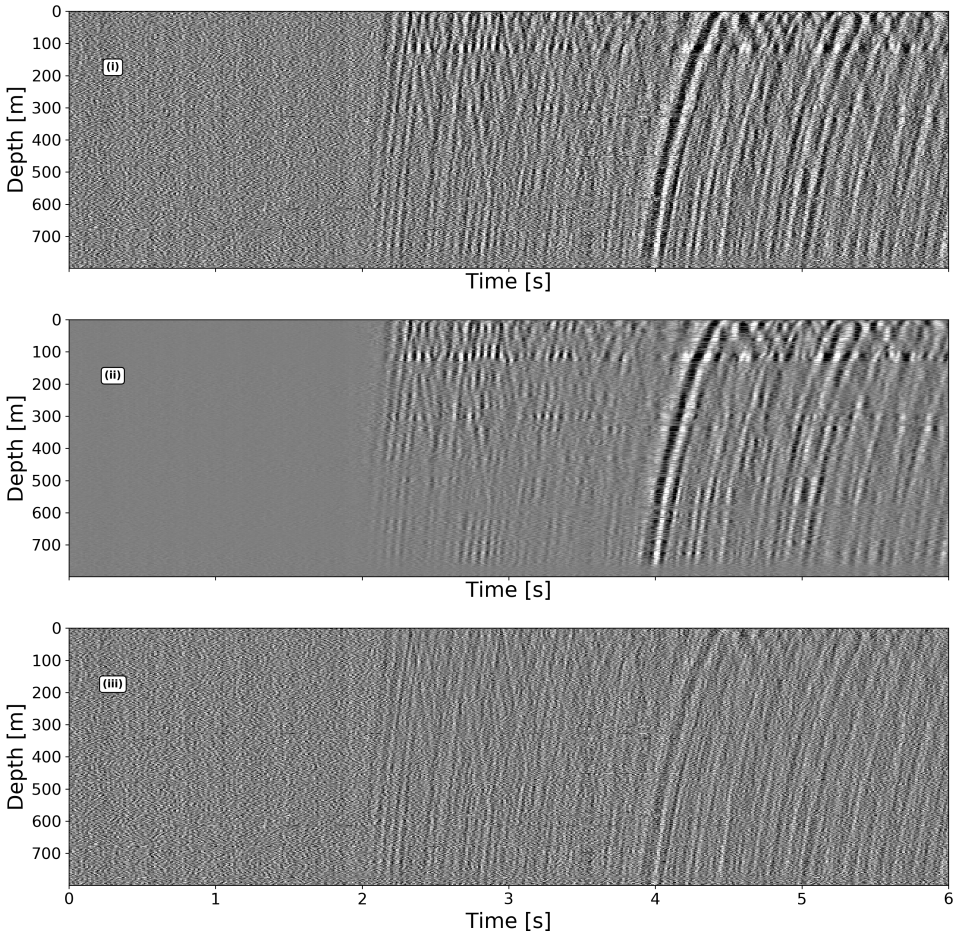

Figure 9: Denoising performance of the U-Net model on event2. The noisy signal is plotted in panel (i). Panel (ii) shows the denoised signal. The recovered noise is shown in panel (iii). We see signal moveout patterns in panel (iii). The leaked signal is weaker compared to that shown in panel (iii) of Figure 11. [CR]

REFERENCES

Ajo-Franklin, J., S. Dou, N. Lindsey, T. M. Daley, B. Freifeld, E. R. Martin, M. Robertson, and C. Ulrich, 2017, Timelapse surface wave monitoring of permafrost thaw using distributed acoustic sensing and a permanent automated seismic source: SEG Technical Program Expanded Abstracts 2017, 5223–5227.

Biondi, B., E. Martin, S. Cole, M. Karrenbach, and N. Lindsey, 2017, Earthquakes analysis using data recorded by the Stanford DAS Array: SEG Technical Program

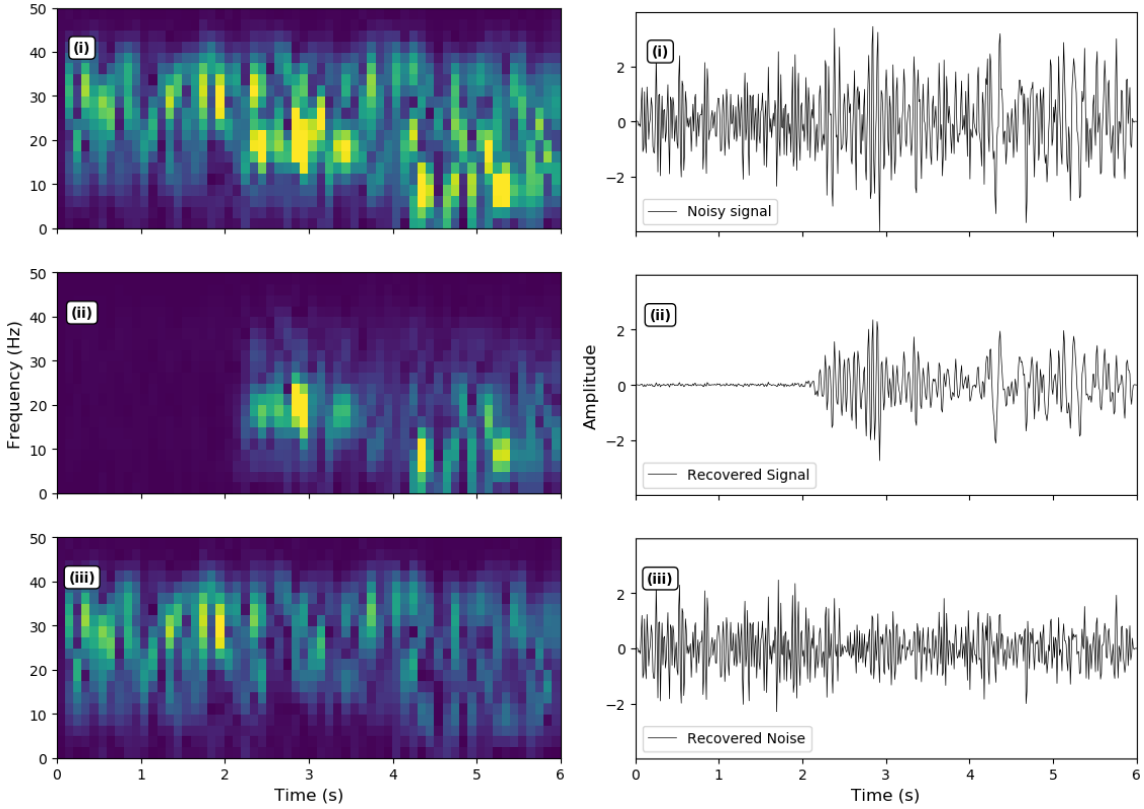

(a) (b)

Figure 10: Denoising performance of Unet1 on event2, trace #100 at a depth of 100 m of seismograph shown in Figure 9. Ground truth clean signal, noise, and noisy signal in time-frequency (a) and time (b) domain are plotted in panels (i) (ii) (iii). Noise is not well recovered after the first arrival (around 1 s). [CR]

Expanded Abstracts, 2752–2756.

Chambolle, A., 2004, An algorithm for total variation minimization and applications: Journal of Mathematical Imaging and Vision, **20**, 89–97.

Daley, T. M., B. M. Freifeld, B. Ajo-Franklin, S. Dou, R. Pevzner, S. Shulakova , Valeriya Kashikar, D. E. Miller, J. Goetz, J. Henninges, and S. Lueth, 2013, Field testing of fiber-optic distributed acoustic sensing (DAS) for subsurface seismic monitoring: The Leading Edge, **32**, 699–706.

Daley, T. M., D. E. Miller, K. Dodds, P. Cook, and B. M. Freifeld, 2016, Field testing of modular borehole monitoring with simultaneous distributed acoustic sensing and geophone vertical seismic profiles at Citronelle, Alabama: Geophysical Prospecting, **64**, 1318–1334.

Dou, S., N. Lindsey, A. M. Wagner, T. M. Daley, B. Freifeld, M. Robertson, J. Peterson, C. Ulrich, E. R. Martin, and J. B. Ajo-Franklin, 2017, Distributed Acoustic Sensing for Seismic Monitoring of the Near Surface: A Traffic-Noise Interferometry Case Study: Scientific Reports, **7**, 1–12.

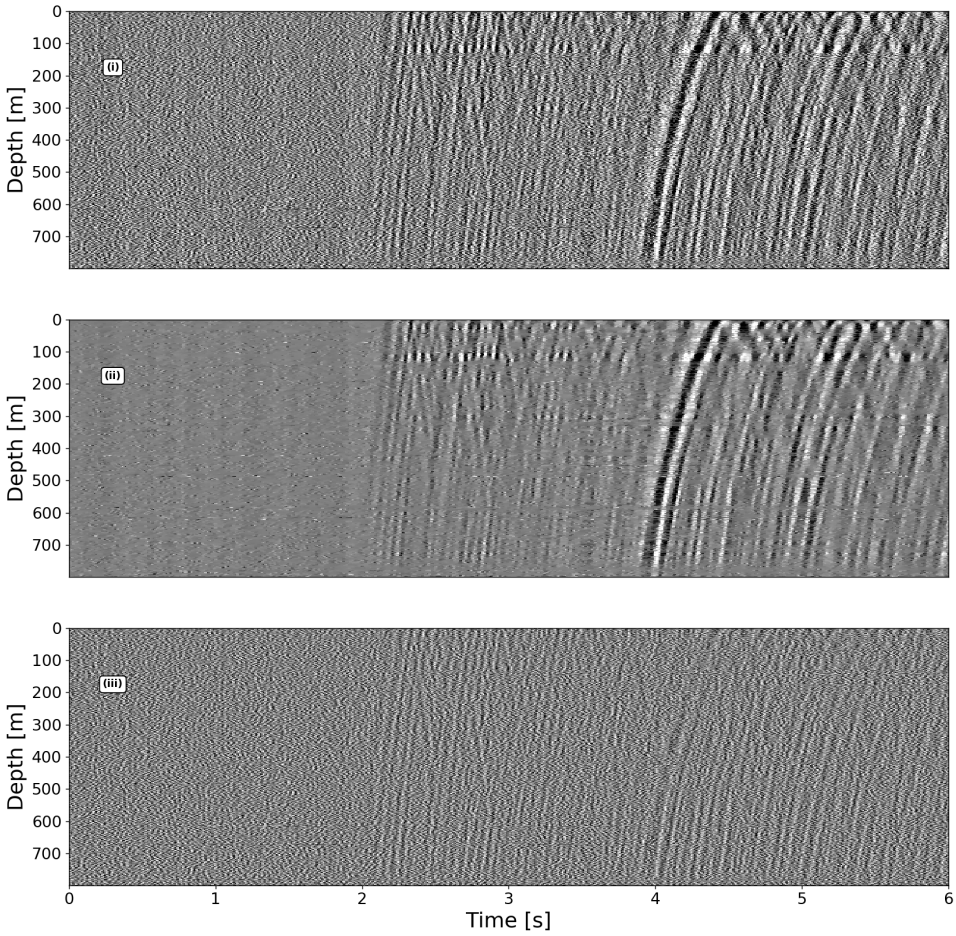

Figure 11: Denoising performance of the total variation method on a event2. The noisy signal is plotted in panel (i). Panel (ii) shows the denoised signal. The recovered noise is shown in panel (iii). We show less noise energy is filtered out in panel (ii), and stronger signal energy is left in panel (iii) compared to Figure 9. [ER]

Hole, J. A., T. Ryberg, G. S. Fuis, F. Bleibinhaus, and A. K. Sharma, 2006, Structure of the San Andreas fault zone at SAFOD from a seismic refraction survey: Geophysical Research Letters, **33**, L07312.

Hornman, J. C., 2017, Field trial of seismic recording using distributed acoustic sensing with broadside sensitive fibre-optic cables: Geophysical Prospecting, **65**, 35–46.

Jousset, P., T. Reinsch, T. Ryberg, H. Blanck, A. Clarke, R. Aghayev, G. P. Hersir, J. Henninges, M. Weber, and C. M. Krawczyk, 2018, Dynamic strain determination

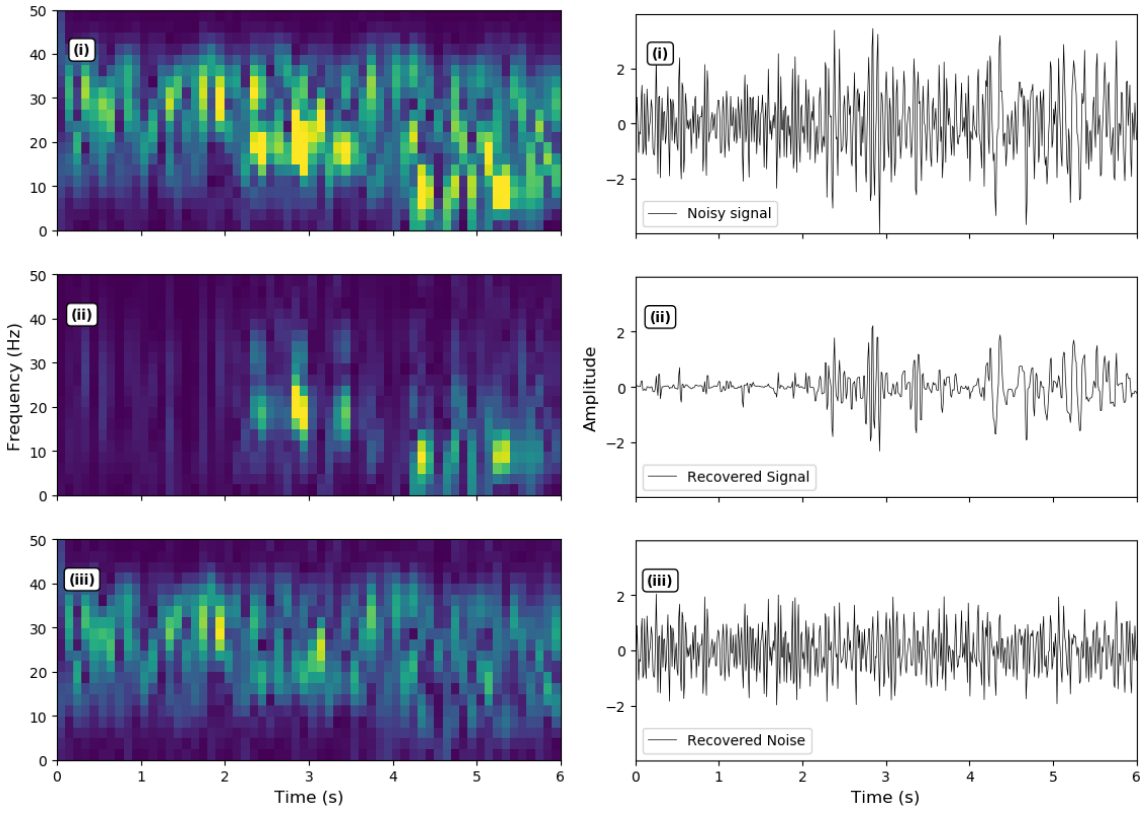

(a) (b)

Figure 12: Denoising performance of the total variation method on event2, trace #100 at a depth of 100 m of seismograph shown in Figure 11. Ground truth clean signal, noise, and noisy signal in time-frequency (a) and time (b) domain are plotted in panels (i) (ii) (iii). Compared to Figure 10, we can see that our network does better at preserving earthquake waveforms and removing noise from a single trace. [CR]

using fibre-optic cables allows imaging of seismological and structural features: Nature Communications, **9**, 2509–2519.

Karrenbach, M., D. Kahn, S. Cole, A. Ridge, K. Boone, J. Rich, K. Silver, and D. Langton, 2017, Hydraulic-fracturing-induced strain and microseismic using in situ distributed fiber-optic sensing: The Leading Edge, **36**, 837–844.

Lellouch, A., S. Yuan, Z. Spica, B. Biondi, and W. Ellsworth, 2019, A moveout-based method for the detection of weak seismic events using downhole DAS arrays: Presented at the 81st EAGE Conference & Exhibition.

Lindsey, N. J., E. R. Martin, D. S. Dreger, B. Freifeld, S. Cole, S. R. James, B. L. Biondi, and J. B. Ajo-Franklin, 2017, Fiber-Optic Network Observations of Earthquake Wavefields: Geophysical Research Letters, **44**, 792–799.

Martin, E., B. Biondi, M. Karrenbach, and S. Cole, 2017a, Ambient Noise Interferometry from DAS Array in Underground Telecommunications Conduits: Presented at the 79th EAGE Conference & Exhibition.

Martin, E. R., and B. L. Biondi, 2018, Eighteen Months of Continuous Near-surface Monitoring with DAS Data Collected Under Stanford University: SEG Technical Program Expanded Abstracts 2018, 4958–4962.

Martin, E. R., C. M. Castillo, S. Cole, P. S. Sawasdee, S. Yuan, R. Clapp, M. Karrenbach, and B. L. Biondi, 2017b, Seismic monitoring leveraging existing telecom infrastructure at the SDASA : Active , passive , and ambient-noise analysis: The Leading Edge, **36**, 1025–1031.

Mateeva, A., J. Lopez, J. Mestayer, P. Wills, B. Cox, D. Kiyashchenko, Z. Yang, W. Berlang, R. Detomo, and S. Grandi, 2013, Distributed acoustic sensing for reservoir monitoring with VSP: The Leading Edge, **32**, 3–7.

Mateeva, A., J. Lopez, H. Potters, J. Mestayer, B. Cox, D. Kiyashchenko, P. Wills, S. Grandi, K. Hornman, B. Kuvshinov, W. Berlang, Z. Yang, and R. Detomo, 2014, Distributed acoustic sensing for reservoir monitoring with vertical seismic profiling: Geophysical Prospecting, **62**, 679–692.

Ronneberger, O., P. F. Fischer, and T. Brox, 2015, Seismic Signal Denoising and Decomposition Using Deep Neural Networks: Presented at the International Conference on Medical image computing and computer-assisted intervention, Springer, Cham.

Wang, H. F., X. Zeng, D. E. Miller, D. Fratta, K. L. Feigl, C. H. Thurber, and R. J. Mellors, 2018, Ground motion response to an ML 4.3 earthquake using co-located distributed acoustic sensing and seismometer arrays: Geophysical Journal International, **213**, 2020–2036.

Zhu, W., S. M. Mousavi, and G. C. Beroza, 2018, Seismic Signal Denoising and Decomposition Using Deep Neural Networks: arXiv preprint.

Zoback, M., S. Hickman, and W. Ellsworth, 2011, Scientific drilling into the San Andreas fault zone - An overview of SAFOD's first five years: Scientific Drilling, **22**, 14–28.